

A *Priori* Error Estimates for Some Discontinuous Galerkin Immersed Finite Element Methods^{*†}

Tao Lin[‡] Qing Yang[§] Xu Zhang[¶]

Abstract

In this paper, we derive *a priori* error estimates for a class of interior penalty discontinuous Galerkin (DG) methods using immersed finite element (IFE) functions for a classic second-order elliptic interface problem. The error estimation shows that these methods can converge optimally in a mesh-dependent energy norm. The combination of IFEs and DG formulation in these methods allows local mesh refinement in the Cartesian mesh structure for interface problems. Numerical results are provided to demonstrate the convergence and local mesh refinement features of these DG-IFE methods.

1 Introduction

Let Ω be a rectangular domain in \mathbb{R}^2 , and let $\Gamma \subset \Omega$ be a smooth curve separating Ω into two subdomains Ω^- and Ω^+ with $\Omega^- \cap \Omega^+ = \emptyset$ (see the first plot in Figure 1). We consider the following typical elliptic interface problem

$$-\nabla \cdot (\beta \nabla u) = f, \quad \text{in } \Omega^+ \cup \Omega^-, \quad (1.1)$$

$$u = 0, \quad \text{on } \partial\Omega, \quad (1.2)$$

where the diffusion coefficient β is a positive piecewise constant function:

$$\beta(X) = \begin{cases} \beta^-, & X \in \Omega^-, \\ \beta^+, & X \in \Omega^+. \end{cases} \quad (1.3)$$

According to the conservation laws, the following jump conditions are required on the interface:

$$[[u]]_{\Gamma} = 0, \quad (1.4)$$

$$\left[\left[\beta \frac{\partial u}{\partial \mathbf{n}} \right] \right]_{\Gamma} = 0. \quad (1.5)$$

Interface problems arise in many applications where mathematical simulations are carried out in a domain containing multiple materials. The elliptic interface problem (1.1) - (1.5) considered in this article appears frequently because the involved differential equation captures many basic physical phenomena. A wide variety of numerical methods have been developed for interface problems, among which the finite element methods are advantageous for their capability to handle simulation domains with complicated geometry. It is well-known that conventional finite element methods generally require the mesh to fit the

^{*}Key words: immersed finite element, discontinuous Galerkin, Cartesian mesh, interface problems, local mesh refinement

[†]This work is partially supported by NSF grant DMS-1016313

[‡]Department of Mathematics, Virginia Tech, Blacksburg, VA 24061, tlin@math.vt.edu

[§]School of Mathematical Science, Shandong Normal University, Jinan 250014, P. R. China

[¶]Department of Mathematics, Purdue University, West Lafayette, IN, 47907, xuzhang@purdue.edu

interface geometry (see the second plot in Figure 1); otherwise, the convergence cannot be guaranteed [3, 6, 10]. However, for a problem with a complicated material interface, constructing a satisfactory body-fitting mesh is often costly, and this burden becomes more severe if the simulation involves a moving interface [21, 31, 35] because the mesh has to be generated repeatedly according to each interface location to be considered. In addition, some simulations, such as the particle-in-cell (PIC) method [5, 24, 40], can be carried out more efficiently on structured/Cartesian meshes. Due to these reasons, a wide variety of numerical methods based on Cartesian meshes have been developed. For an overview of these methods, we refer to [14, 15, 23, 27, 33, 34] and the references therein.

Immersed finite element (IFE) methods were recently introduced for solving interface problems. The main feature of IFE methods is that they can use meshes independent of the interface location, *i.e.*, they allow interface to cut through the interior of elements in a mesh (see the last two plots in Figure 1). Hence, Cartesian (triangular or rectangular) meshes can be preferably employed in IFE methods to solve interface problems. We refer the readers to [11, 25, 26, 28, 29] for more features about IFE methods based on triangular meshes, and [17, 19, 30, 39] for IFE methods based on rectangular meshes. We note that IFE methods in these literatures are applied in the continuous Galerkin formulation.

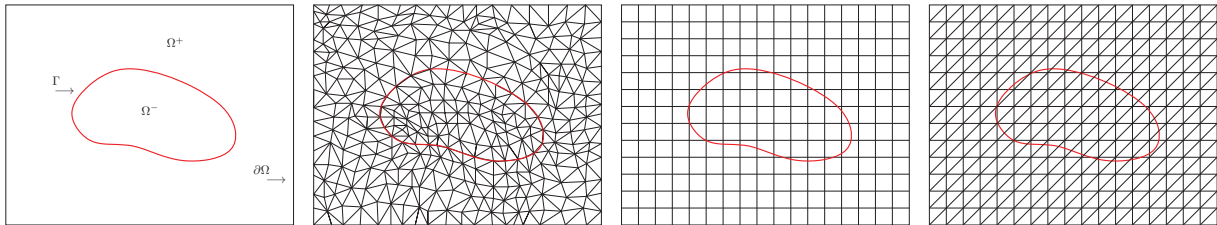


Figure 1: from left: a simulation domain, a body-fitting triangular mesh, a non-body-fitting Cartesian mesh, and a non-body-fitting triangular mesh.

The discontinuous Galerkin (DG) methods for elliptic boundary value problems can be traced back to 1970s (see [4, 36]) and they become increasingly popular recently as indicated by these survey articles and books [2, 12, 22, 37]. Because there is no continuity imposed on the approximating function across the element boundary, DG methods can locally perform h -, p -, and hp -refinement flexibly and efficiently. For elliptic and parabolic equations, the interior penalty DG (IPDG) methods [1, 13, 38, 41] are well understood and widely used. The main feature of IPDG methods is that penalty terms are added on interior edges to stabilize the bilinear form of the scheme, so that the linear system is positive definite. In [16, 18], the IFE and IPDG ideas were combined together for solving interface problems on Cartesian meshes with local refinement capability. To alleviate the issue of higher degrees of freedom in usual DG formulation, authors in [20] considered the so-called *selective* DG-IFE methods that employ DG formulation in selected elements while using the usual Galerkin formulation in the rest of the solution domain. Numerical examples have demonstrated that these DG-IFE methods can converge optimally, and our goal in this article is to theoretically establish the optimal *a priori* error estimates for DG-IFE methods that were discussed in [16, 18, 20].

The rest of the paper is organized as follows. In Section 2, we recall the DG-IFE methods originally proposed in [16, 18]. In Section 3, we present *a priori* error estimates for these DG-IFE methods. An error estimate in a mesh-dependant energy norm is derived, and this error estimate is optimal according to the polynomials used in the IFE spaces. In Section 4, numerical experiments are provided to demonstrate features of DG-IFE methods. Brief conclusions are given in Section 5.

2 Discontinuous Galerkin Immersed Finite Element Methods

In this paper, we adopt notations and norms of usual Sobolev spaces. For $r > 1$ and any subset $G \subseteq \Omega$ that is cut through by Γ , we use the following function spaces:

$$\tilde{H}^r(G) = \{v \in H^1(G) : v|_{G \cap \Omega^s} \in H^r(G \cap \Omega^s), s = + \text{ or } -\}, \quad \tilde{H}_0^r(G) = \tilde{H}^r(G) \cap H_0^1(G),$$

equipped with the norm

$$\|v\|_{\tilde{H}^r(G)}^2 = \|v\|_{H^r(G \cap \Omega^-)}^2 + \|v\|_{H^r(G \cap \Omega^+)}^2, \quad \forall v \in \tilde{H}^r(G).$$

From now on, we use C with or without subscripts to denote generic positive constants, possibly different at different occurrences, but they are independent of the mesh size and interface.

Let $\{\mathcal{T}_h\}$ with $0 < h < 1$ be a family of triangular or rectangular Cartesian meshes of Ω . An element cut through by the interface is called an interface element; otherwise, it is called a non-interface element. For each mesh \mathcal{T}_h , we let \mathcal{T}_h^i be the set of interface elements of \mathcal{T}_h and \mathcal{T}_h^n be the set of non-interface elements. We denote by \mathcal{E}_h the set of edges of \mathcal{T}_h . Also, let \mathcal{E}_h^i and \mathcal{E}_h^b be the set of interior edges and boundary edges of \mathcal{T}_h , respectively. Similarly, if an edge is cut through by the interface, it is called an interface edge; otherwise, it is called a non-interface edge. Let \mathcal{E}_h^i and \mathcal{E}_h^n be the set of interface edges and non-interface edges, respectively. Moreover, we use $\mathring{\mathcal{E}}_h^i$ and $\mathring{\mathcal{E}}_h^n$ to denote the set of interior interface edges and interior non-interface edges, respectively. Without loss of generality, we assume that elements in \mathcal{T}_h satisfy the following conditions:

- (H1) If one edge of an element meets Γ at more than one point, then this edge is part of Γ .
- (H2) If Γ meets the boundary of an element at two points, then these two points must be on different edges of this element.

For every interface element $K \in \mathcal{T}_h^i$, we assume its boundary intersects with the interface Γ at points D and E . Then, the line segment \overline{DE} divides K into two sub-elements K^+ and K^- with $K = K^+ \cup K^- \cup \overline{DE}$. With a given mesh \mathcal{T}_h on Ω , we define the following broken Sobolev spaces:

$$\begin{aligned} \tilde{H}^2(\mathcal{T}_h) = \{v \in L^2(\Omega) : & \forall K \in \mathcal{T}_h^n, v|_K \in H^2(K); \\ & \forall K \in \mathcal{T}_h^i, v|_K \in H^1(K), \quad v|_{K^s} \in H^2(K^s), s = +, -\}. \end{aligned}$$

and

$$\tilde{H}_0^2(\mathcal{T}_h) = \{v \in \tilde{H}^2(\mathcal{T}_h) : v|_{\partial\Omega} = 0\}.$$

We now recall some standard notations for describing IPDG methods [9, 22, 37]. For each edge B , we associate a unit normal vector \mathbf{n}_B . If $B \in \mathring{\mathcal{E}}_h$, we let $K_{B,1}$ and $K_{B,2}$ be two elements that share B as the common edge and let \mathbf{n}_B be the outward normal with respect to $K_{B,1}$. If $B \in \mathcal{E}_h^b$, \mathbf{n}_B is taken to be the unit outward vector normal to $\partial\Omega$. For a function u defined on $K_{B,1} \cup K_{B,2}$, we denote its average and jump over $B \in \mathring{\mathcal{E}}_h$ by

$$\{\!\!\{u\}\!\!\}_B = \frac{1}{2}((u|_{K_{B,1}})|_B + (u|_{K_{B,2}})|_B), \quad \llbracket u \rrbracket_B = (u|_{K_{B,1}})|_B - (u|_{K_{B,2}})|_B.$$

If B is a boundary edge, we set

$$\{\!\!\{u\}\!\!\}_B = \llbracket u \rrbracket_B = u|_B.$$

For simplicity, we usually drop the subscript B from these notations if there is no danger to cause any confusion.

To obtain a variational form for the interface problem (1.1) - (1.5), we multiply (1.1) by a test function $v \in \tilde{H}_0^2(\mathcal{T}_h)$, integrate both sides on each element $K \in \mathcal{T}_h$, and apply the Green's formula to have

$$\int_K \beta \nabla u \cdot \nabla v dX - \int_{\partial K} \beta \nabla u \cdot \mathbf{n}_K v ds = \int_K f v dX. \quad (2.1)$$

Note that (2.1) holds regardless whether K is a non-interface element or an interface element. For $K \in \mathcal{T}_h^n$, the derivation follows from the standard procedure. When K is an interface element, (2.1) follows from applying the Green's formula piecewisely over sub-elements of K determined according to the smoothness of u and v , then summing up over K and applying the flux continuity (1.5). Summarizing (2.1) over all elements we obtain

$$\sum_{K \in \mathcal{T}_h} \int_K \beta \nabla u \cdot \nabla v dX - \sum_{B \in \hat{\mathcal{E}}_h} \int_B \{\{\beta \nabla u \cdot \mathbf{n}_B\}\} \llbracket v \rrbracket ds = \int_{\Omega} f v dX. \quad (2.2)$$

Since the solution u is continuous almost everywhere in Ω , we can assume

$$\epsilon \sum_{B \in \hat{\mathcal{E}}_h} \int_B \{\{\beta \nabla v \cdot \mathbf{n}_B\}\} \llbracket u \rrbracket ds = 0, \quad \sum_{B \in \hat{\mathcal{E}}_h} \frac{\sigma_B^0}{|B|^\alpha} \int_B \llbracket u \rrbracket \llbracket v \rrbracket ds = 0, \quad (2.3)$$

for any constants $\epsilon, \alpha > 0$, and $\sigma_B^0 \geq 0$. Here $|B|$ denotes the length of B . Adding the two terms in (2.3) to (2.2), we obtain the weak form of interface problem (1.1) - (1.5): Find $u \in \tilde{H}_0^2(\Omega)$ such that

$$a_\epsilon(u, v) = (f, v), \quad \forall v \in \tilde{H}_0^2(\mathcal{T}_h), \quad (2.4)$$

where the bilinear form $a_\epsilon(\cdot, \cdot): H_h(\Omega) \times H_h(\Omega) \rightarrow \mathbb{R}$ is

$$\begin{aligned} a_\epsilon(w, v) &= \sum_{K \in \mathcal{T}_h} \int_K \beta \nabla w \cdot \nabla v dX - \sum_{B \in \hat{\mathcal{E}}_h} \int_B \{\{\beta \nabla w \cdot \mathbf{n}_B\}\} \llbracket v \rrbracket ds \\ &\quad + \epsilon \sum_{B \in \hat{\mathcal{E}}_h} \int_B \{\{\beta \nabla v \cdot \mathbf{n}_B\}\} \llbracket w \rrbracket ds + \sum_{B \in \hat{\mathcal{E}}_h} \frac{\sigma_B^0}{|B|^\alpha} \int_B \llbracket w \rrbracket \llbracket v \rrbracket ds, \end{aligned} \quad (2.5)$$

and $H_h(\Omega) = \tilde{H}_0^2(\Omega) + \tilde{H}_0^2(\mathcal{T}_h)$. The weak form derived here for the interface problem (1.1)-(1.5) is in the same format as the standard weak form used in DG finite element methods for the usual elliptic boundary value problems [9, 22, 37]. As suggested by DG finite element methods, the parameter ϵ is usually chosen as $-1, 0$, or 1 . Note that the bilinear form $a_\epsilon(\cdot, \cdot)$ is symmetric if $\epsilon = -1$ and is nonsymmetric otherwise.

We now introduce the IFE approximation of the broken space $\tilde{H}_0^2(\mathcal{T}_h)$. For every element $K \in \mathcal{T}_h$, denote by $A_i, i = 1, \dots, d_K$, the vertices of K . Here $d_K = 3$ or $d_K = 4$ depending on whether K is a triangular or rectangular element. On each non-interface element $K \in \mathcal{T}_h^n$, we let $\psi_i, i = 1, \dots, d_K$ be the standard linear or bilinear finite element nodal basis associated with the vertex A_i of K . The local FE space on $K \in \mathcal{T}_h^n$ is defined as

$$S_h(K) = \text{span}\{\psi_i : 1 \leq i \leq d_K\}.$$

On an interface element $K \in \mathcal{T}_h^i$, we let $\phi_i, i = 1, \dots, d_K$ be the linear [28, 29] or bilinear [17, 30] IFE nodal basis associated with vertex A_i . We let local IFE space on $K \in \mathcal{T}_h^i$ be

$$S_h(K) = \text{span}\{\phi_i : 1 \leq i \leq d_K\}.$$

Then, we define the discontinuous IFE space over the mesh \mathcal{T}_h as follows:

$$S_h(\mathcal{T}_h) = \{v \in L^2(\Omega) : v|_K \in S_h(K)\}, \quad \mathring{S}_h(\mathcal{T}_h) = \{v \in S_h(\mathcal{T}_h) : v|_{\partial\Omega} = 0\}.$$

One can easily see that $\mathring{S}_h(\mathcal{T}_h)$ is a subspace of $H_h(\Omega)$.

Finally, we state the DG-IFE methods for the interface problem (1.1) - (1.5) as: Find $u_h \in \mathring{S}_h(\mathcal{T}_h)$ such that

$$a_\epsilon(u_h, v_h) = (f, v_h), \quad \forall v_h \in \mathring{S}_h(\mathcal{T}_h). \quad (2.6)$$

3 A Priori Error Estimation

In this section, we derive *a priori* error estimates for the DG-IFE methods (2.6) in an energy norm $\|\cdot\|_h : H_h(\Omega) \rightarrow \mathbb{R}$ defined as follows

$$\|v\|_h = \left(\sum_{K \in \mathcal{T}_h} \int_K \beta \nabla v \cdot \nabla v dX + \sum_{B \in \mathcal{E}_h} \frac{\sigma_B^0}{|B|^\alpha} \int_B \llbracket v \rrbracket \llbracket v \rrbracket ds \right)^{1/2}. \quad (3.1)$$

We first present a few lemmas required in the error analysis. By the standard scaling argument, one can show the following trace inequalities [37]:

Lemma 3.1. (*Standard trace inequalities*) *Let K be a triangle or rectangle with diameter h_K , and B be an edge of K . There exists a constant C such that*

$$\|v\|_{L^2(B)} \leq C|B|^{1/2}|K|^{-1/2}(\|v\|_{L^2(K)} + h_K\|\nabla v\|_{L^2(K)}), \quad \forall v \in H^1(K), \quad (3.2)$$

$$\|\nabla v\|_{L^2(B)} \leq C|B|^{1/2}|K|^{-1/2}(\|\nabla v\|_{L^2(K)} + h_K\|\nabla^2 v\|_{L^2(K)}), \quad \forall v \in H^2(K), \quad (3.3)$$

where $\nabla^2 v$ is the Hessian of v .

On an interface element $K \in \mathcal{T}_h^i$, we recall from [29, 30] that the local IFE space $S_h(K) \subset H^1(K)$. This implies that the trace inequality (3.2) is valid for $v \in S_h(K)$. However, since $S_h(K) \not\subset H^2(K)$ for $K \in \mathcal{T}_h^i$ in general, the second inequality (3.3) cannot be applied to functions in $S_h(K)$. Nevertheless, in [32, 42], this trace inequality has been extended to IFE functions. We recall this result in the following lemma.

Lemma 3.2. (*Trace inequalities for IFE functions*) *Let \mathcal{T}_h be a Cartesian triangular or rectangular mesh and let $K \in \mathcal{T}_h$ be an interface triangle or rectangle with diameter h_K and let B be an edge of K . There exists a constant C , independent of interface location but depending on the jump of the coefficient β , such that for every linear or bilinear IFE function v defined on K , the following inequality hold*

$$\|\beta \nabla v \cdot \mathbf{n}_B\|_{L^2(B)} \leq Ch_K^{-1/2} \|\sqrt{\beta} \nabla v\|_{L^2(K)}. \quad (3.4)$$

We now describe the interpolation with IFE functions. For $K \in \mathcal{T}_h^n$, the local interpolation operator is defined as $I_{h,K}^n : C(K) \rightarrow S_h(K)$:

$$I_{h,K}^n u(X) = \sum_{i=1}^{d_K} u(A_i) \psi_i(X), \quad K \in \mathcal{T}_h^n.$$

For $K \in \mathcal{T}_h^i$, the local interpolation operator is defined as $I_{h,K}^i : C(K) \rightarrow S_h(K)$:

$$I_{h,K}^i u(X) = \sum_{i=1}^{d_K} u(A_i) \phi_i(X), \quad K \in \mathcal{T}_h^i.$$

On each non-interface element, we have the standard approximation theory for the finite element interpolation:

$$\|u - I_{h,K}^n u\|_{L^2(K)} + h_K |u - I_{h,K}^n u|_{H^1(K)} \leq Ch_K^2 |u|_{H^2(K)}, \quad \forall K \in \mathcal{T}_h^n. \quad (3.5)$$

On each interface element, the approximation property of the IFE interpolation proved in [17, 29] provides similar error bounds as follows:

$$\|u - I_{h,K}^i u\|_{L^2(K)} + h_K |u - I_{h,K}^i u|_{H^1(K)} \leq Ch_K^2 \|u\|_{\tilde{H}^2(K)}, \quad \forall K \in \mathcal{T}_h^i, \quad (3.6)$$

where the constant C is independent of interface location. For $u \in \tilde{H}^2(\Omega)$, let $I_h : \tilde{H}^2(\Omega) \rightarrow S_h(\mathcal{T}_h)$ be the interpolation defined by

$$(I_h u)|_K = \begin{cases} I_{h,K}^n u, & K \in \mathcal{T}_h^n, \\ I_{h,K}^i u, & K \in \mathcal{T}_h^i. \end{cases} \quad (3.7)$$

Multiplying h_K^{-1} on both sides of (3.5) and (3.6), then summing up for all non-interface and interface elements, we can obtain an interpolation error bound on the domain Ω as stated in the next lemma.

Lemma 3.3. *For $u \in \tilde{H}^2(\Omega)$, satisfying the interface jump conditions (1.4) and (1.5), there exists a constant C such that*

$$\left(\sum_{K \in \mathcal{T}_h} h_K^{-2} \|u - I_h u\|_{L^2(K)}^2 \right)^{1/2} + \left(\sum_{K \in \mathcal{T}_h} |u - I_h u|_{H^1(K)}^2 \right)^{1/2} \leq Ch \|u\|_{\tilde{H}^2(\Omega)}, \quad (3.8)$$

where $h = \max_{K \in \mathcal{T}_h} h_K$.

The following lemma provides the approximation property of $I_h u$ in the energy norm $\|\cdot\|_h$.

Lemma 3.4. *Assume $\alpha \leq 1$ in the energy norm (3.1). For every $u \in \tilde{H}^2(\Omega)$, satisfying the interface jump conditions (1.4) and (1.5), there exists a constant C such that*

$$\|u - I_h u\|_h \leq Ch \|u\|_{\tilde{H}^2(\Omega)}. \quad (3.9)$$

Proof. By the definition of $\|\cdot\|_h$, we have

$$\|u - I_h u\|_h^2 = \sum_{K \in \mathcal{T}_h} \int_K \beta |\nabla(u - I_h u)|^2 dX + \sum_{B \in \tilde{\mathcal{E}}_h} \frac{\sigma_B^0}{|B|^\alpha} \| [u - I_h u] \|_{L^2(B)}^2. \quad (3.10)$$

For the first term on the right hand side, we use the estimate (3.8) to have

$$\sum_{K \in \mathcal{T}_h} \int_K \beta |\nabla(u - I_h u)|^2 dX \leq \beta_{max} \sum_{K \in \mathcal{T}_h} \|\nabla(u - I_h u)\|_{L^2(K)}^2 \leq \beta_{max} h^2 \|u\|_{\tilde{H}^2(\Omega)}^2 \quad (3.11)$$

where $\beta_{max} = \max\{\beta^-, \beta^+\}$. Now we bound the second term in (3.10). Using the standard trace equality (3.2) and the approximation properties (3.5) or (3.6), we have

$$\begin{aligned} \frac{\sigma_B^0}{|B|^\alpha} \| [u - I_h u] \|_{L^2(B)}^2 &\leq \frac{\sigma_B^0}{|B|^\alpha} (\|(u - I_h u)|_{K_{B,1}}\|_{L^2(B)}^2 + \|(u - I_h u)|_{K_{B,2}}\|_{L^2(B)}^2) \\ &\leq Ch_{K_{B,1}}^{-1-\alpha} \left(\|u - I_h u\|_{L^2(K_{B,1})}^2 + h_{K_{B,1}}^2 \|\nabla(u - I_h u)\|_{L^2(K_{B,1})}^2 \right) \\ &\quad + Ch_{K_{B,2}}^{-1-\alpha} \left(\|u - I_h u\|_{L^2(K_{B,2})}^2 + h_{K_{B,2}}^2 \|\nabla(u - I_h u)\|_{L^2(K_{B,2})}^2 \right) \\ &\leq Ch_{K_{B,1}}^{3-\alpha} \|u\|_{V(K_{B,1})}^2 + Ch_{K_{B,2}}^{3-\alpha} \|u\|_{V(K_{B,2})}^2 \\ &\leq Ch^{3-\alpha} \left(\|u\|_{V(K_{B,1})}^2 + \|u\|_{V(K_{B,2})}^2 \right), \end{aligned}$$

where $V(K) = H^2(K)$ for $K \in \mathcal{T}_h^n$ and $V(K) = \tilde{H}^2(K)$ for $K \in \mathcal{T}_h^i$, and $h = \max_{K \in \mathcal{T}_h} h_K$. Also, the second inequality is due to the shape-regular property of Cartesian triangular or rectangular meshes $h_{K_{B,i}} \leq C|B|$, $i = 1, 2$. Thus, for $\alpha \leq 1$, we get

$$\sum_{B \in \tilde{\mathcal{E}}_h} \frac{\sigma_B^0}{|B|^\alpha} \| [u - I_h u] \|_{L^2(B)}^2 \leq Ch^2 \|u\|_{\tilde{H}^2(\Omega)}^2. \quad (3.12)$$

Finally, combining (3.11) and (3.12), we get (3.9). \square

The coercivity of the bilinear form $a_\epsilon(\cdot, \cdot)$ is analyzed in the following lemma.

Lemma 3.5. *There exists a constant $\kappa > 0$ such that*

$$a_\epsilon(v_h, v_h) \geq \kappa \|v_h\|_h^2, \quad \forall v_h \in \mathring{S}_h(\mathcal{T}_h) \quad (3.13)$$

holds for $\epsilon = 1$ unconditionally and holds for $\epsilon = 0$ or -1 under the conditions that the penalty parameter σ_B^0 is large enough and $\alpha \geq 1$.

Proof. From the definition of $a_\epsilon(\cdot, \cdot)$, we have

$$a_\epsilon(v_h, v_h) = \sum_{K \in \mathcal{T}_h} \int_K \beta |\nabla v_h|^2 dX + (\epsilon - 1) \sum_{B \in \dot{\mathcal{E}}_h} \int_B \{\{\beta \nabla v_h \cdot \mathbf{n}_B\}\} \llbracket v_h \rrbracket ds + \sum_{B \in \dot{\mathcal{E}}_h} \frac{\sigma_B^0}{|B|^\alpha} \int_B \llbracket v_h \rrbracket^2 ds. \quad (3.14)$$

We first note that, when $\epsilon = 1$, the coercivity follows directly from (3.14) and the definition of $\|\cdot\|_h$. If $\epsilon = 0$ or -1 , we need to bound the second term on the right hand side of (3.14). For each $B \in \dot{\mathcal{E}}_h$, recall that $K_{B,i} \in \mathcal{T}_h$, $i = 1, 2$ are two elements sharing B as their common edge. If $K_{B,i}$, $i = 1$ or 2 is a non-interface element, by the trace inequality (3.3) and inverse inequalities, we have

$$\begin{aligned} \|(\beta \nabla v_h \cdot \mathbf{n}_B)|_{K_{B,i}}\|_{L^2(B)} &\leq \beta_{\max} \|(\nabla v_h)|_{K_{B,i}}\|_{L^2(B)} \\ &\leq C \beta_{\max} h_{K_{B,i}}^{-\frac{1}{2}} \|\nabla v_h\|_{L^2(K_{B,i})} \\ &\leq C \frac{\beta_{\max}}{\sqrt{\beta_{\min}}} h_{K_{B,i}}^{-\frac{1}{2}} \|\sqrt{\beta} \nabla v_h\|_{L^2(K_{B,i})}, \end{aligned} \quad (3.15)$$

where $\beta_{\min} = \min\{\beta^-, \beta^+\}$, and $\beta_{\max} = \max\{\beta^-, \beta^+\}$. Then, using the assumption that $\alpha \geq 1$ and by either the estimate (3.15) or IFE trace inequality (3.4) depending on whether the element is a non-interface element or an interface element, we have

$$\begin{aligned} \int_B \{\{\beta \nabla v_h \cdot \mathbf{n}_B\}\} \llbracket v_h \rrbracket ds &\leq \| \{\{\beta \nabla v_h \cdot \mathbf{n}_B\}\} \|_{L^2(B)} \| \llbracket v_h \rrbracket \|_{L^2(B)} \\ &\leq \frac{1}{2} (\|(\beta \nabla v_h \cdot \mathbf{n}_B)|_{K_{B,1}}\|_{L^2(B)} + \|(\beta \nabla v_h \cdot \mathbf{n}_B)|_{K_{B,2}}\|_{L^2(B)}) \| \llbracket v_h \rrbracket \|_{L^2(B)} \\ &\leq \frac{C}{2} \left(h_{K_{B,1}}^{-\frac{1}{2}} \|\sqrt{\beta} \nabla v_h\|_{L^2(K_{B,1})} + h_{K_{B,2}}^{-\frac{1}{2}} \|\sqrt{\beta} \nabla v_h\|_{L^2(K_{B,2})} \right) \| \llbracket v_h \rrbracket \|_{L^2(B)} \\ &\leq C \left(\|\sqrt{\beta} \nabla v_h\|_{L^2(K_{B,1})}^2 + \|\sqrt{\beta} \nabla v_h\|_{L^2(K_{B,2})}^2 \right)^{\frac{1}{2}} \frac{1}{|B|^{\alpha/2}} \| \llbracket v_h \rrbracket \|_{L^2(B)}. \end{aligned}$$

Summing over all interior edges and using the Young's inequality, we have

$$\begin{aligned} &\sum_{B \in \dot{\mathcal{E}}_h} \int_B \{\{\beta \nabla v_h \cdot \mathbf{n}_B\}\} \llbracket v_h \rrbracket ds \\ &\leq C \sum_{B \in \dot{\mathcal{E}}_h} \left(\|\sqrt{\beta} \nabla v_h\|_{L^2(K_{B,1})}^2 + \|\sqrt{\beta} \nabla v_h\|_{L^2(K_{B,2})}^2 \right)^{1/2} \frac{1}{|B|^{\alpha/2}} \| \llbracket v_h \rrbracket \|_{L^2(B)} \\ &\leq C \left(\sum_{B \in \dot{\mathcal{E}}_h} \frac{1}{|B|^\alpha} \| \llbracket v_h \rrbracket \|_{L^2(B)}^2 \right)^{1/2} \left(\sum_{B \in \dot{\mathcal{E}}_h} \left(\|\sqrt{\beta} \nabla v_h\|_{L^2(K_{B,1})}^2 + \|\sqrt{\beta} \nabla v_h\|_{L^2(K_{B,2})}^2 \right) \right)^{1/2} \\ &\leq \frac{\delta}{2} \sum_{K \in \mathcal{T}_h} \|\sqrt{\beta} \nabla v_h\|_{L^2(K)}^2 + \frac{C}{2\delta} \sum_{B \in \dot{\mathcal{E}}_h} \frac{1}{|B|^\alpha} \| \llbracket v_h \rrbracket \|_{L^2(B)}^2. \end{aligned} \quad (3.16)$$

Then, for $\epsilon = 0$, we can choose

$$\delta = 1 \quad \text{and} \quad \sigma_B^0 > \frac{C}{2},$$

and for $\epsilon = -1$, we can choose

$$\delta = \frac{1}{2} \quad \text{and} \quad \sigma_B^0 > 2C.$$

Substituting these parameters in (3.16) and then putting it in (3.14), we obtain (3.13). \square

We also need an error bound for the IFE interpolation $I_h u$ on interface edges which has been proved in [32]. We present the result in the following lemma.

Lemma 3.6. For every $u \in \tilde{H}^3(\Omega)$, satisfying the interface jump conditions (1.4) and (1.5), there exists a constant C independent of interface location such that

$$\|\beta(\nabla(u - I_h u))|_K \cdot \mathbf{n}_B\|_{L^2(B)}^2 \leq C \left(h_K^2 \|u\|_{\tilde{H}^3(\Omega)}^2 + h_K \|u\|_{\tilde{H}^2(K)}^2 \right), \quad (3.17)$$

where K is an interface element and B is one of its interface edge.

The assumptions of α in Lemma 3.4 and Lemma 3.5 suggest that we should choose $\alpha = 1$ in our DG formulation (2.6). Now we are ready to prove the *a priori* error estimate for DG-IFE method (2.6).

Theorem 3.1. Let $u \in \tilde{H}^3(\Omega)$ be the exact solution to the interface problem (1.1) to (1.5) and $u_h \in S_h(\mathcal{T}_h)$ be the solution to (2.6) with $\alpha = 1$, $\epsilon = -1, 0$, or 1 . Then there exists a constant C such that

$$\|u - u_h\|_h \leq Ch \|u\|_{\tilde{H}^3(\Omega)}. \quad (3.18)$$

Proof. Subtracting the weak form (2.4) from the DG-IFE scheme (2.6), we get

$$a_\epsilon(u - u_h, v_h) = 0, \quad \forall v_h \in \dot{S}_h(\mathcal{T}_h). \quad (3.19)$$

For every $w_h \in \dot{S}_h(\mathcal{T}_h)$, using (3.19) and the coercivity (3.13), we have

$$\begin{aligned} \kappa \|u_h - w_h\|_h^2 &\leq a_\epsilon(u_h - w_h, u_h - w_h) = a_\epsilon(u - w_h, u_h - w_h) \\ &\leq \left| \sum_{K \in \mathcal{T}_h} \int_K \beta \nabla(u - w_h) \cdot \nabla(u_h - w_h) dX \right| + \left| \sum_{B \in \dot{\mathcal{E}}_h} \int_B \{\beta \nabla(u - w_h) \cdot \mathbf{n}_B\} \llbracket u_h - w_h \rrbracket ds \right| \\ &\quad + \left| \sum_{B \in \dot{\mathcal{E}}_h} \int_B \{\beta \nabla(u_h - w_h) \cdot \mathbf{n}_B\} \llbracket u - w_h \rrbracket ds \right| + \left| \sum_{B \in \dot{\mathcal{E}}_h} \frac{\sigma_B^0}{|B|^\alpha} \int_B \llbracket u - w_h \rrbracket \llbracket u_h - w_h \rrbracket ds \right| \\ &\triangleq T_1 + T_2 + T_3 + T_4. \end{aligned} \quad (3.20)$$

We proceed to bound the terms $T_i, i = 1, 2, 3, 4$ in (3.20). By the Cauchy-Schwarz inequality and Young's inequality with parameter $\delta > 0$, we can easily bound T_1 and T_2 :

$$\begin{aligned} T_1 &\leq \left(\sum_{K \in \mathcal{T}_h} \|\sqrt{\beta} \nabla(u - w_h)\|_{L^2(K)}^2 \right)^{1/2} \left(\sum_{K \in \mathcal{T}_h} \|\sqrt{\beta} \nabla(u_h - w_h)\|_{L^2(K)}^2 \right)^{1/2} \\ &\leq \frac{1}{4\delta} \beta_{\max} \|\nabla(u - w_h)\|_{L^2(\Omega)}^2 + \delta \sum_{K \in \mathcal{T}_h} \|\sqrt{\beta} \nabla(u_h - w_h)\|_{L^2(K)}^2 \\ &\leq C(\delta) \|\nabla(u - w_h)\|_{L^2(\Omega)}^2 + \delta \|u_h - w_h\|_h^2, \end{aligned} \quad (3.21)$$

and

$$\begin{aligned} T_2 &\leq C(\delta) \sum_{B \in \dot{\mathcal{E}}_h} \frac{|B|^\alpha}{\sigma_B^0} \|\{\beta \nabla(u - w_h) \cdot \mathbf{n}_B\}\|_{L^2(B)}^2 + \delta \sum_{B \in \dot{\mathcal{E}}_h} \frac{\sigma_B^0}{|B|^\alpha} \|\llbracket u_h - w_h \rrbracket\|_{L^2(B)}^2 \\ &\leq C(\delta) \sum_{B \in \dot{\mathcal{E}}_h} \frac{|B|^\alpha}{\sigma_B^0} \|\{\beta \nabla(u - w_h) \cdot \mathbf{n}_B\}\|_{L^2(B)}^2 + \delta \|u_h - w_h\|_h^2, \end{aligned} \quad (3.22)$$

where $C(\delta)$ emphasizes that this is a constant depending on δ . For T_3 , by the Cauchy-Schwarz inequality we have

$$T_3 \leq \sum_{B \in \dot{\mathcal{E}}_h} \|\{\beta \nabla(u_h - w_h) \cdot \mathbf{n}_B\}\|_{L^2(B)} \|\llbracket u - w_h \rrbracket\|_{L^2(B)}. \quad (3.23)$$

First, using the standard trace equality (3.2), we have

$$\begin{aligned} \|\llbracket u - w_h \rrbracket\|_{L^2(B)} &\leq \|(u - w_h)|_{K_{B,1}}\|_{L^2(B)} + \|(u - w_h)|_{K_{B,2}}\|_{L^2(B)} \\ &\leq Ch_{K_{B,1}}^{-1/2} (\|u - w_h\|_{L^2(K_{B,1})} + h_{K_{B,1}} \|\nabla(u - w_h)\|_{L^2(K_{B,1})}) \\ &\quad + Ch_{K_{B,2}}^{-1/2} (\|u - w_h\|_{L^2(K_{B,2})} + h_{K_{B,2}} \|\nabla(u - w_h)\|_{L^2(K_{B,2})}). \end{aligned}$$

Then, by the trace inequalities (3.3) or (3.4), we have

$$\|\{\beta \nabla(u_h - w_h) \cdot \mathbf{n}_B\}\|_{L^2(B)} \leq C \left(h_{K_{B,1}}^{-1/2} \|\sqrt{\beta} \nabla(u_h - w_h)\|_{L^2(K_{B,1})} + h_{K_{B,2}}^{-1/2} \|\sqrt{\beta} \nabla(u_h - w_h)\|_{L^2(K_{B,2})} \right).$$

Substituting the above two bounds into (3.23) and applying Young's inequality, we obtain

$$T_3 \leq C(\delta) \left(\sum_{K \in \mathcal{T}_h} h_K^{-2} \|u - w_h\|_{L^2(K)}^2 + \sum_{K \in \mathcal{T}_h} \|\nabla(u - w_h)\|_{L^2(K)}^2 \right) + \delta \|u_h - w_h\|_h^2. \quad (3.24)$$

For T_4 , we use the assumption $\alpha = 1$, the Cauchy-Schwarz inequality, and Young's inequality to have

$$T_4 \leq \sum_{B \in \dot{\mathcal{E}}_h} \left(\frac{1}{4\delta} \frac{\sigma_B^0}{|B|} \int_B \llbracket u - w_h \rrbracket \llbracket u - w_h \rrbracket ds + \delta \frac{\sigma_B^0}{|B|} \int_B \llbracket u_h - w_h \rrbracket \llbracket u_h - w_h \rrbracket ds \right). \quad (3.25)$$

Again, by trace inequality (3.2), we have

$$\begin{aligned} \frac{\sigma_B^0}{|B|} \int_B \llbracket u - w_h \rrbracket^2 ds &\leq C \frac{\sigma_B^0}{|B|} \left(\|(u - w_h)|_{K_{B,1}}\|_{L^2(B)}^2 + \|(u - w_h)|_{K_{B,2}}\|_{L^2(B)}^2 \right) \\ &\leq Ch_{K_{B,1}}^{-2} (\|u - w_h\|_{L^2(K_{B,1})} + h_{K_{B,1}} \|\nabla(u - w_h)\|_{L^2(K_{B,1})})^2 \\ &\quad + Ch_{K_{B,2}}^{-2} (\|u - w_h\|_{L^2(K_{B,2})} + h_{K_{B,2}} \|\nabla(u - w_h)\|_{L^2(K_{B,2})})^2. \end{aligned} \quad (3.26)$$

Using (3.26) in (3.25), we have

$$T_4 \leq C(\delta) \left(\sum_{K \in \mathcal{T}_h} h_K^{-2} \|u - w_h\|_{L^2(K)}^2 + \sum_{K \in \mathcal{T}_h} \|\nabla(u - w_h)\|_{L^2(K)}^2 \right) + \delta \|u_h - w_h\|_h^2. \quad (3.27)$$

Substituting (3.21), (3.22), (3.24) and (3.27) into (3.20) and choosing $\delta = \kappa/8$, we obtain

$$\begin{aligned} \|u_h - w_h\|_h^2 &\leq C \sum_{K \in \mathcal{T}_h} \|\nabla(u - w_h)\|_{L^2(K)}^2 + C \sum_{B \in \dot{\mathcal{E}}_h} \frac{|B|}{\sigma_B^0} \|\{\beta \nabla(u - w_h) \cdot \mathbf{n}_B\}\|_{L^2(B)}^2 \\ &\quad + C \sum_{K \in \mathcal{T}_h} h_K^{-2} \|u - w_h\|_{L^2(K)}^2 \end{aligned} \quad (3.28)$$

Now, we let w_h be the IFE interpolation $I_h u$ in (3.28) and use the optimal approximation capability of linear or bilinear DG-IFE spaces (3.8) to have

$$\|u_h - I_h u\|_h^2 \leq Ch^2 \|u\|_{\dot{H}^2(\Omega)}^2 + Ch \sum_{B \in \dot{\mathcal{E}}_h} \sum_{i=1,2} \|(\beta \nabla(u - I_h u) \cdot \mathbf{n}_B)|_{K_{B,i}}\|_{L^2(B)}^2. \quad (3.29)$$

We now bound the second term on the right hand side of (3.29). If $K_{B,i}$, $i = 1$ or 2 is a non-interface element, we use the trace inequality (3.3) to obtain

$$\begin{aligned} \|(\beta \nabla(u - I_h u) \cdot \mathbf{n}_B)|_{K_{B,i}}\|_{L^2(B)}^2 &\leq C(h_{K_{B,i}}^{-1} \|\nabla(u - I_h u)\|_{L^2(K_{B,i})} + h_{K_{B,i}} \|\nabla^2 u\|_{L^2(K_{B,i})})^2 \\ &\leq Ch_{K_{B,i}} \|u\|_{\dot{H}^2(K_{B,i})}^2. \end{aligned} \quad (3.30)$$

If $K_{B,i}$ is an interface element, we use (3.17) to get

$$\|(\beta \nabla(u - I_h u) \cdot \mathbf{n}_B)|_{K_{B,i}}\|_{L^2(B)}^2 \leq C \left(h_{K_{B,i}}^2 \|u\|_{\tilde{H}^3(\Omega)}^2 + h_{K_{B,i}} \|u\|_{\tilde{H}^2(K_{B,i})}^2 \right). \quad (3.31)$$

Due to the shape regularity of mesh \mathcal{T}_h , we have the following bound on the union of interface elements

$$\sum_{K \in \mathcal{T}_h^i} h_K^2 \|u\|_{\tilde{H}^3(\Omega)}^2 \leq h \|u\|_{\tilde{H}^3(\Omega)}^2 \sum_{K \in \mathcal{T}_h^i} h_K \leq Ch \|u\|_{\tilde{H}^3(\Omega)}^2. \quad (3.32)$$

Summing up the estimates (3.30) and (3.31) over all interior edges, and using the bound in (3.32), we obtain

$$\sum_{B \in \mathcal{E}_h} \sum_{i=1,2} \|(\beta \nabla(u - I_h u) \cdot \mathbf{n}_B)|_{K_{B,i}}\|_{L^2(B)}^2 \leq Ch \|u\|_{\tilde{H}^3(\Omega)}^2 + Ch \|u\|_{\tilde{H}^2(\Omega)}^2 \leq Ch \|u\|_{\tilde{H}^3(\Omega)}^2. \quad (3.33)$$

Then, substituting (3.33) to (3.29) we obtain

$$\|u_h - I_h u\|_h \leq Ch \|u\|_{\tilde{H}^3(\Omega)}. \quad (3.34)$$

Finally, the error estimate (3.18) follows from triangle inequality, (3.34) and (3.9). \square

Remark 3.1. *The DG-IFE methods proposed in this article and their related error estimation can be extended to arbitrary shape-regular unstructured interface independent meshes.*

Remark 3.2. *The proof of Theorem 3.1 requires that the solution is piecewise H^3 , which is higher than the usual piecewise H^2 assumption imposed on methods using a finite element space based on linear polynomials. Consequently, our error estimate here is optimal according to the rate of convergence expected from linear polynomials but not with respect to the regularity of solution space.*

4 Numerical Examples

In this section, we present numerical examples to demonstrate features of interior penalty DG-IFE methods for elliptic interface problems. Let the solution domain Ω be the open rectangle $(-1, 1) \times (-1, 1)$ and let the interface Γ be the ellipse centered at $(x_0, y_0) = (-0.2, 0.1)$ with semi-axes $a = \frac{\pi}{6.28}$, $b = \frac{3}{2}a$. The interface separates Ω into two sub-domains, denoted by Ω^- and Ω^+ , *i.e.*,

$$\Omega^- = \{(x, y) : r(x, y) < 1\}, \quad \text{and} \quad \Omega^+ = \{(x, y) : r(x, y) > 1\},$$

where

$$r(x, y) = \sqrt{\frac{(x - x_0)^2}{a^2} + \frac{(y - y_0)^2}{b^2}}.$$

The exact solution u to the interface problem is chosen as follows

$$u(x, y) = \begin{cases} a^2 b^2 \frac{r^p}{\beta^-}, & \text{if } (x, y) \in \Omega^-, \\ a^2 b^2 \left(\frac{r^p}{\beta^+} + \frac{1}{\beta^-} - \frac{1}{\beta^+} \right), & \text{if } (x, y) \in \Omega^+. \end{cases} \quad (4.1)$$

Here p is a parameter and we choose $p = 5$ in Examples 1 - 3 representing a solution with enough regularity, and $p = 0.5$ in Example 4 representing a solution with low regularity. Note that this solution does not satisfy the homogeneous boundary condition (1.2). We use this function for numerical verification because both the algorithm and the analysis in Section 2 and Section 3 can be extended to the nonhomogeneous boundary condition case via a standard treatment.

Example 1: In this example, we present a group of numerical results for demonstrating the convergence of the DG-IFE methods on Cartesian triangular meshes. Additional numerical results on

rectangular meshes are provided in [16, 18, 20]. Specifically, the Cartesian triangular meshes $\{\mathcal{T}_h, h > 0\}$ are formed by first partitioning Ω into $N \times N$ congruent squares of size $h = 2/N$ and then dividing each rectangle into two congruent triangles with one of its diagonal lines.

First, we consider the case in which $(\beta^-, \beta^+) = (1, 10)$ representing a moderate discontinuity in the diffusion coefficient across the interface. The symmetric DG-IFE scheme is employed to solve the interface problem with parameters $\alpha = 1$ and $\sigma_B^0 = 1000$ for all interior edges. Errors of numerical solutions in the L^∞ , L^2 , and semi- H^1 norms are reported in Table 1. For comparison, we also solve the same interface problem using the continuous Galerkin linear IFE method [28, 29] on the same meshes, and the corresponding numerical results are listed in Table 2.

N	$\ \cdot\ _{L^\infty}$	rate	$\ \cdot\ _{L^2}$	rate	$ \cdot _{H^1}$	rate
10	$2.8333E-2$		$3.7991E-2$		$6.7917E-1$	
20	$8.4503E-3$	1.7454	$9.3605E-3$	2.0210	$3.4653E-1$	0.9708
40	$2.5075E-3$	1.7527	$2.3062E-3$	2.0210	$1.7456E-1$	0.9893
80	$7.2318E-4$	1.7938	$5.6970E-4$	2.0173	$8.7630E-2$	0.9942
160	$2.0134E-4$	1.8447	$1.4140E-4$	2.0105	$4.3903E-2$	0.9971
320	$5.4720E-5$	1.8795	$3.5178E-5$	2.0070	$2.1972E-2$	0.9986
640	$1.4450E-5$	1.9210	$8.7729E-6$	2.0035	$1.0991E-2$	0.9994
1280	$3.7496E-6$	1.9463	$2.1903E-6$	2.0019	$5.4965E-3$	0.9997

Table 1: Errors of linear DG-IFE solutions with $\beta^- = 1$, $\beta^+ = 10$, $\sigma_B^0 = 1000$.

N	$\ \cdot\ _{L^\infty}$	rate	$\ \cdot\ _{L^2}$	rate	$ \cdot _{H^1}$	rate
10	$2.8619E-2$		$4.4051E-2$		$6.7876E-1$	
20	$1.1416E-2$	1.3259	$1.1333E-2$	1.9587	$3.4808E-1$	0.9635
40	$5.3027E-3$	1.1062	$2.8882E-3$	1.9722	$1.7641E-1$	0.9805
80	$1.9396E-3$	1.4510	$7.3078E-4$	1.9827	$8.9155E-2$	0.9845
160	$1.0689E-3$	0.8596	$1.8726E-4$	1.9644	$4.5387E-2$	0.9740
320	$5.4774E-4$	0.9646	$5.1220E-5$	1.8702	$2.3305E-2$	0.9617
640	$2.7498E-4$	0.9942	$1.6771E-5$	1.6107	$1.2277E-2$	0.9247
1280	$1.4113E-4$	0.9623	$7.1759E-6$	1.2248	$6.7321E-3$	0.8668

Table 2: Errors of the classic Galerkin IFE solutions with $\beta^- = 1$, $\beta^+ = 10$.

The data in Table 1 clearly demonstrate that the convergence rate of the DG-IFE method in the semi- H^1 norm is optimal which corroborates the *a priori* error estimates (3.18) for DG-IFE methods since the semi- H^1 norm is part of the energy norm. In addition, the data in this table indicate that the convergence rate of the DG-IFE method in the L^2 norm is also optimal. However, from Table 2, we can see that the convergence rates of the Galerkin IFE solution in the L^2 and H^1 norms start to deteriorate when the mesh size becomes smaller than $h = 2/320$. This comparison indicates that the DG-IFE methods are more stable than the continuous Galerkin IFE method.

Next we consider the case involving a larger discontinuity in the diffusion coefficient, *i.e.*, $\beta^- = 1$, and $\beta^+ = 1000$. We use nonsymmetric DG-IFE scheme for this experiment and choose $\sigma_B^0 = 1000$ for all interior edges. As demonstrated by the data in Table 3, the DG-IFE solutions converge optimally in the L^2 and semi- H^1 norms.

Example 2: From Tables 1 and 2, it is interesting to note that errors in the DG-IFE solutions gauged in L^∞ norm are much smaller than those in the classic Galerkin IFE solutions when the mesh size is

N	$\ \cdot\ _{L^\infty}$	rate	$\ \cdot\ _{L^2}$	rate	$ \cdot _{H^1}$	rate
10	$1.9381E-2$		$1.5338E-2$		$2.1012E-1$	
20	$1.2420E-2$	0.6420	$6.0704E-3$	1.3373	$1.3141E-1$	0.6772
40	$4.0332E-3$	1.6227	$1.4957E-3$	2.0210	$6.9522E-2$	0.9185
80	$9.9934E-4$	2.0129	$3.6124E-4$	2.0498	$3.5490E-2$	0.9701
160	$2.7965E-4$	1.8374	$8.9863E-5$	2.0072	$1.7949E-2$	0.9835
320	$8.0700E-5$	1.7930	$2.1864E-5$	2.0392	$9.0223E-3$	0.9924
640	$2.2017E-5$	1.8740	$5.3914E-6$	2.0198	$4.5229E-3$	0.9963
1280	$5.9615E-6$	1.8848	$1.3343E-6$	2.0146	$2.2641E-3$	0.9983

Table 3: Errors of linear DG-IFE solutions with $\beta^- = 1$, $\beta^+ = 1000$, $\sigma_B^0 = 1000$.

small enough. It has been observed that the classic IFE solution has a so called ‘‘crown’’ shortcoming as demonstrated by the plot on the left side of Figure 2, meaning its point-wise accuracy is much worse in the vicinity of the interface than the rest of the solution domain. We think this severity of inaccuracy is caused by the discontinuity in the IFE functions across the interface edges. Nevertheless, the DG-IFE methods contain penalty terms that can alleviate the adverse impacts from the discontinuity across element edges, especially those from interface edges. Therefore, DG-IFE methods can usually outperform the classic Galerkin IFE method around the interface as demonstrated by the plot on the right side of Figure 2. IFE solutions in these plots are generated on a mesh formed by partitioning Ω into 160×160 congruent rectangles first, then generating triangular elements by the diagonal line of these rectangles.

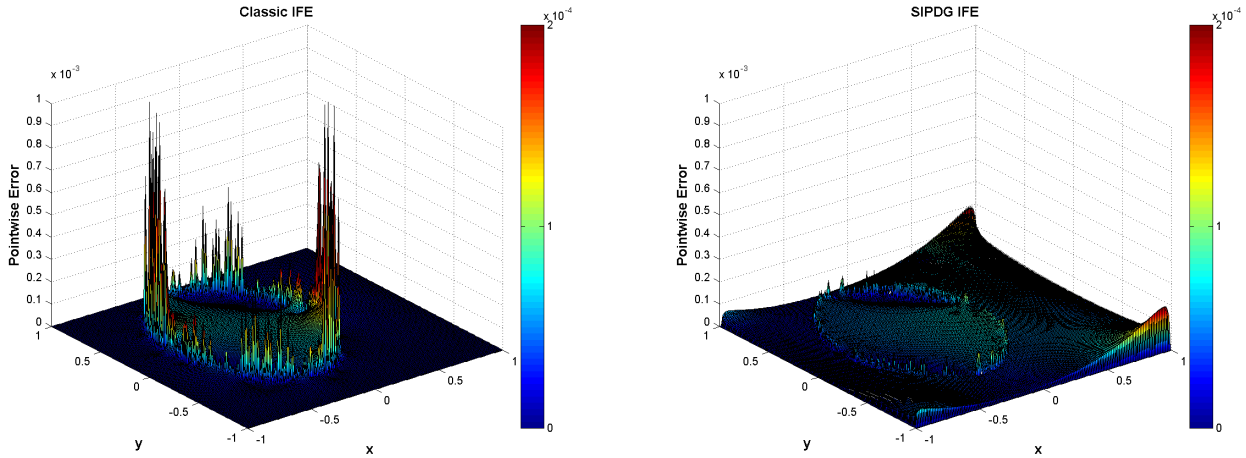


Figure 2: Point-wise error of Galerkin IFE solution and DG-IFE solution.

Example 3: One desirable feature of the DG formulation is the local adaptivity in mesh or polynomials because this formulation does not require the inter-element continuity of finite element functions. The combination of IFE spaces and the DG formulation leads to a new class of finite element methods that allow local mesh refinement while maintaining the possibility of using the desirable structured Cartesian meshes for solving problems with nontrivial interface geometry. This example is for demonstrating this feature of the DG-IFE methods.

The discontinuity in the coefficient of the interface problem limits the smoothness of the exact solution around interface. The low regularity of the solution around interface usually has an adverse

impact on the accuracy of the numerical solution around the interface. To overcome this challenge, one can employ more finite element functions around the interface and a way to achieve this is to refine interface elements. To demonstrate this idea, we consider the same example described above for a larger coefficient jump ($\beta^- = 1$, $\beta^+ = 1000$). We start with a uniform Cartesian mesh $\mathcal{T}_h^{(0)}$ consisting of 10×10 rectangles. For $k \geq 1$, the mesh $\mathcal{T}_h^{(k)}$ is generated by refining the previous mesh $\mathcal{T}_h^{(k-1)}$ via cutting each of its interface elements into four congruent rectangles by connecting midpoints on opposite edges. We then solve the interface problem (1.1) - (1.5) on a sequence of 6 such meshes generated by the refinement procedure described above using the nonsymmetric DG-IFE method with $\sigma_B^0 = 1000$ on all internal edges. Errors in the L^∞ , L^2 , and semi- H^1 norms generated on each mesh are presented in Table 4. In the second column, $|\mathcal{T}_h^{(k)}|$ denotes the number of elements in the mesh $\mathcal{T}_h^{(k)}$. The numbers of degrees of freedom are listed in the third column. The initial mesh $\mathcal{T}_h^{(0)}$ and the refined meshes $\mathcal{T}_h^{(2)}$ and $\mathcal{T}_h^{(4)}$ are illustrated in Figure 3.

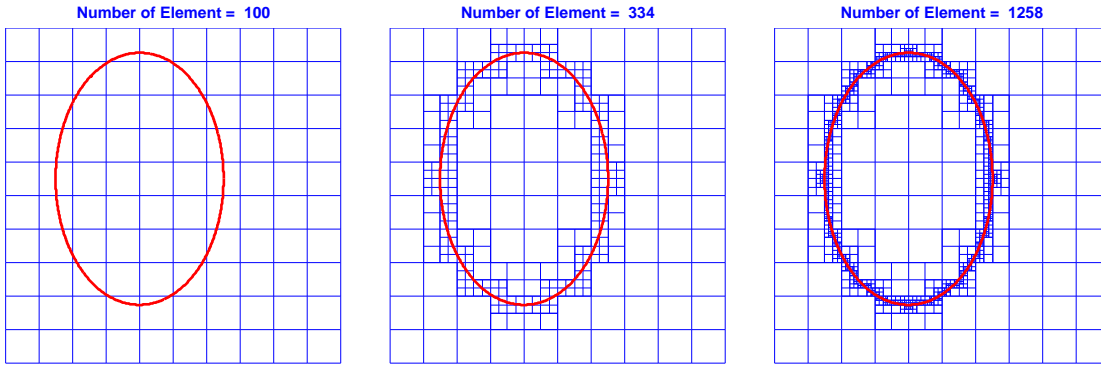


Figure 3: Solution meshes $\mathcal{T}_h^{(0)}$, $\mathcal{T}_h^{(2)}$, and $\mathcal{T}_h^{(4)}$.

Mesh	$ \mathcal{T}_h^{(i)} $	DoF	$\ \cdot\ _{L^\infty}$	$\ \cdot\ _{L^2}$	$ \cdot _{H^1}$
$\mathcal{T}_h^{(0)}$	100	400	1.5064E-2	1.5667E-2	1.9393E-1
$\mathcal{T}_h^{(1)}$	178	712	1.9242E-2	8.7358E-3	1.5041E-1
$\mathcal{T}_h^{(2)}$	334	1336	1.2799E-2	5.9608E-3	1.2761E-1
$\mathcal{T}_h^{(3)}$	646	2584	1.2789E-2	5.7452E-3	1.2321E-1
$\mathcal{T}_h^{(4)}$	1258	5032	1.2484E-2	5.6245E-3	1.2233E-1
$\mathcal{T}_h^{(5)}$	2470	9880	1.2431E-2	5.5988E-3	1.2213E-1
$\mathcal{T}_h^{(6)}$	4882	19528	1.2424E-2	5.5940E-3	1.2209E-1

Table 4: Errors of NIPDG-IFE solutions on meshes with local refinement

The data in Table 4 show that the global error in the L^2 and semi- H^1 norms are significantly reduced in the first two steps of local mesh refinements. But further refinements performed on interface elements do not reduce the global error as much as the first two steps. We believe this is because, after the first two refinements, errors of the DG-IFE solutions over non-interface elements become more significant. To further increase the accuracy of DG-IFE solutions, refinement on non-interface elements is also necessary. To demonstrate this idea, we simulate an adaptive local mesh refinement over the whole solution domain. Since *a posteriori* error estimators for IFE methods are not available yet, we use the actual error as the “ideal” error indicator to guide the local refinement just for a proof of concept.

We start from a uniform Cartesian mesh $\mathcal{T}_h^{(0)}$ consisting of 10×10 rectangles. For $k \geq 0$, we produce

a DG-IFE solution u_h for the interface problem on the mesh $\mathcal{T}_h^{(k)}$ and compute the local semi- H^1 norm error $|u - u_h|_{H^1(T)}$ on each element of $\mathcal{T}_h^{(k)}$. We sort these local errors from the largest to the smallest and use this order to form the smallest collection $\tilde{\mathcal{T}}_h^{(k)}$ of the first few elements such that

$$\sum_{T \in \tilde{\mathcal{T}}_h^{(k)}} |u - u_h|_{H^1(T)}^2 \geq \theta |u - u_h|_{H^1(\Omega)}^2. \quad (4.2)$$

Then, we generate a new mesh $\mathcal{T}_h^{(k+1)}$ by refining $\mathcal{T}_h^{(k)}$ via cutting each of the elements in $\tilde{\mathcal{T}}_h^{(k)}$ into four congruent rectangles by connecting midpoints on its opposite edges. The computation repeats over the new mesh $\mathcal{T}_h^{(k+1)}$.

We choose $\theta = 0.2$ and conduct adaptive DG-IFE scheme on each locally refined mesh. In Figure 4, we show the initial mesh $\mathcal{T}_h^{(0)}$, the refined meshes $\mathcal{T}_h^{(7)}, \mathcal{T}_h^{(12)}$, and $\mathcal{T}_h^{(17)}$, and errors of the DG-IFE solutions generated on those meshes. From these plots, we can easily see that the global error in the DG-IFE solution is reduced as the local mesh refinement automatically deploys smaller elements at locations needed according to the “ideal” error indicator while maintaining the Cartesian structure of the meshes.

To see the effectiveness of the adaptive DG-IFE methods, we compare the errors in DG-IFE solutions generated via adaptive mesh refinement to errors of DG-IFE solutions generated on uniform meshes with comparable degrees of freedom in Figure 5. The semi- H^1 norm errors presented in the right plot in Figure 5 shows that the magnitude of errors in adaptive DG-IFE method are smaller than in the method with a uniform mesh when their degrees of freedom are comparable. However, the order of convergence for both schemes are optimal by comparing their errors with the reference line of slope $-1/2$ (the same criteria is used in [7]). We note that the exact solution u defined in (4.1) with $p = 5$ is piecewise smooth, *i.e.* $u \in \dot{H}^3(\Omega)$ (see the left plot in Figure 5), although the global regularity is impacted by the discontinuity of the coefficients. The optimal convergence of the numerical solution in uniform mesh refinement confirms our theoretical error estimate (3.18) in Section 3.

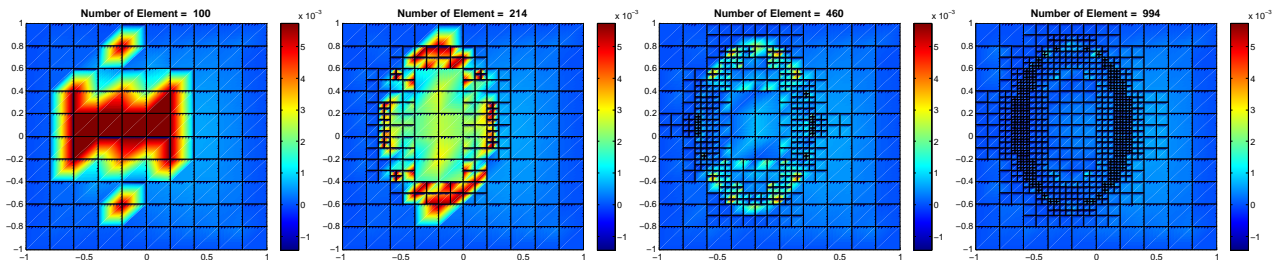


Figure 4: Point-wise error of DG-IFE solutions on meshes: $\mathcal{T}_h^{(0)}$, $\mathcal{T}_h^{(7)}, \mathcal{T}_h^{(12)}$, and $\mathcal{T}_h^{(17)}$

Example 4: In many applications, because of the insufficient regularity in the data, solutions to the involved boundary value problems may not be piecewise smooth enough for a certain convergence theorem to hold. In such cases, finite element or DG methods based on uniform mesh refinement usually fail to converge optimally, but adaptive FE or DG methods with suitably designed mesh refinement strategies can still generate optimally convergent numerical solutions [7, 8]. For interface problems with discontinuous coefficients, the phenomenon is similar. In this example, we demonstrate behaviors of DG-IFE method in adaptive and uniform mesh refinements for solving interface problems whose exact solution has singularity. In particular, this example indicates that the DG-IFE method with adaptive refinement on interface independent meshes can satisfactorily handle interface problems whose exact solutions are less smooth.

We choose the exact solution u in the form of (4.1) with $p = 0.5$ such that it does not satisfy the regularity condition required by Theorem 3.1 on the convergence of the DG-IFE method. This lack of regularity is caused by the singularity of the exact solution at the center of the ellipse as depicted in the

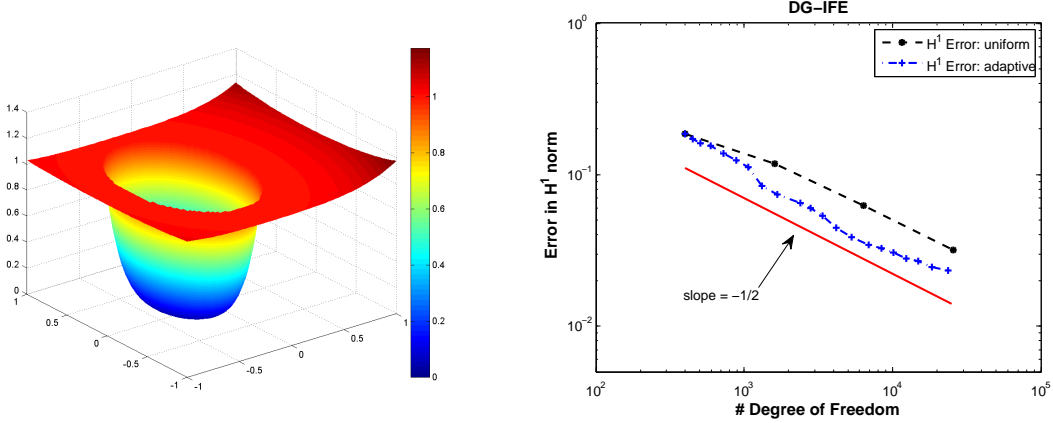


Figure 5: Left: the exact solution u in Example 3. Right: a log-log scale plot of errors of in numerical solutions generated by the adaptive and uniform mesh refinement. The red line with a -0.5 slope is for the reference of optimal convergence.

left plot of Figure 6. The coefficients are set to be $\beta^- = 1$, $\beta^+ = 10$. First, we present the data generated by the DG-IFE method with uniform mesh refinement in Table 5. Specifically, these data are produced by the nonsymmetric DG-IFE method with the penalty $\sigma_B^0 = 100$ on every edge. Errors in L^∞ , L^2 , and semi- H^1 norms are reported, and the convergence rates of the DG-IFE method are obviously not optimal in all three corresponding norms.

N	$\ \cdot\ _{L^\infty}$	rate	$\ \cdot\ _{L^2}$	rate	$ \cdot _{H^1}$	rate
10	$4.2599E-2$		$1.8474E-2$		$1.0415E-1$	
20	$5.7301E-2$	-0.4278	$8.0329E-3$	1.2015	$5.6787E-2$	0.8751
40	$4.5270E-2$	0.3400	$5.5008E-3$	0.5463	$4.2830E-2$	0.4069
80	$3.5386E-2$	0.3554	$3.8353E-3$	0.5203	$3.2011E-2$	0.4201
160	$2.7412E-2$	0.3684	$2.6964E-3$	0.5083	$2.3774E-2$	0.4292
320	$2.1075E-2$	0.3793	$1.9024E-3$	0.5032	$1.7573E-2$	0.4361
640	$1.6098E-2$	0.3886	$1.3441E-3$	0.5012	$1.2940E-2$	0.4415
1280	$1.2237E-2$	0.3967	$9.5014E-4$	0.5005	$9.5021E-3$	0.4461

Table 5: Errors of bilinear nonsymmetric DG-IFE solutions with $p = 0.5$

Next, we report the performance of the adaptive DG-IFE method for solving the same interface problem with this less smooth exact solution. As in Example 3, we use the exact error as an “ideal” error indicator for mesh refinement just for a proof of concept. Starting with a uniform mesh $\mathcal{T}_h^{(0)}$ consisting of 10×10 rectangles, we perform the local mesh refinement based on the same rule as the one in (4.2) with the threshold $\theta = 0.2$. Errors in semi- H^1 norm are depicted in Figure 6, in which, as a comparison, errors from uniform mesh refinement are also plotted. It is obvious that the adaptive DG-IFE method is far more accurate than the DG-IFE method based uniform meshes when their numbers of degrees of freedom are comparable. Moreover, comparing the errors with the reference line of slope $-1/2$, it is obvious that the rate of convergence of the adaptive DG-IFE method is close to optimal from the point view of the degrees of freedom while the rate of convergence of DG-IFE method based on uniform mesh is not optimal. Some meshes in the process of the local refinement are presented in Figure 7 from which one can observe that the refinement is around the center of the ellipse where the exact solution is singular.

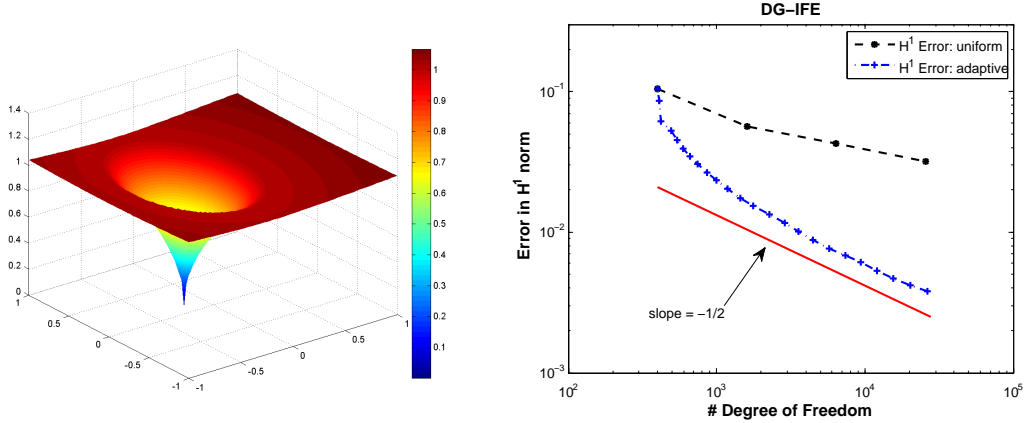


Figure 6: Left: the exact solution u in Example 4. Right: a log-log scale plot of errors of in numerical solutions generated by the adaptive and uniform mesh refinement. The red line with a -0.5 slope is for the reference of optimal convergence.

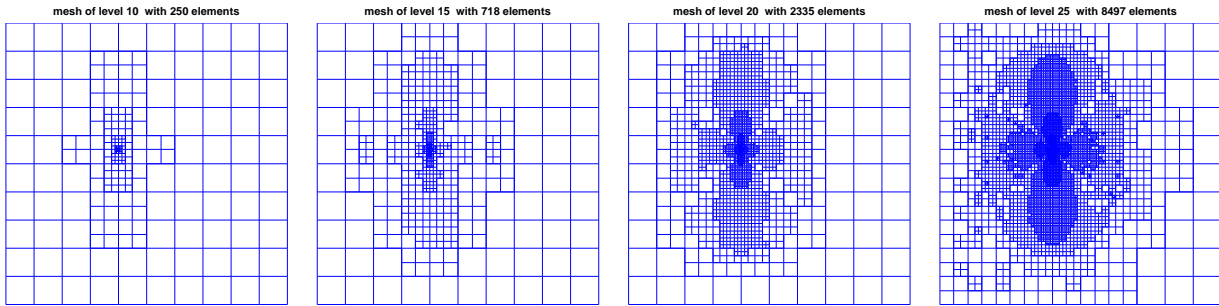


Figure 7: Solution meshes: $\mathcal{T}_h^{(10)}$, $\mathcal{T}_h^{(15)}$, $\mathcal{T}_h^{(20)}$, and $\mathcal{T}_h^{(25)}$

5 Conclusion

In this article, we establish *a priori* error estimates for interior penalty discontinuous Galerkin methods with immersed finite element functions for elliptic interface problem. The method can be used on Cartesian meshes that are independent of the interface. The analysis here shows that the order of convergence of these DG-IFE methods is optimal in the energy norm from the point of the polynomial degree in the finite element spaces. With the enhanced stability, these DG-IFE methods outperform the classic Galerkin IFE methods, especially in vicinity of the interface across which the exact solution is usually less smooth. The proposed DG-IFE schemes allow efficient local mesh refinement while preserving the Cartesian structure of meshes provided that *a posteriori* error estimators are available.

Acknowledgement

The authors would like to thank anonymous referees whose comments and suggestions enhanced the presentation of our research work.

References

- [1] D. N. Arnold. An interior penalty finite element method with discontinuous elements. *SIAM J. Numer. Anal.*, 19(4):742–760, 1982.

- [2] D. N. Arnold, F. Brezzi, B. Cockburn, and L. D. Marini. Unified analysis of discontinuous Galerkin methods for elliptic problems. *SIAM J. Numer. Anal.*, 39(5):1749–1779, 2001/02.
- [3] I. Babuška and J. E. Osborn. Can a finite element method perform arbitrarily badly? *Math. Comp.*, 69(230):443–462, 2000.
- [4] I. Babuška and M. Zlámal. Nonconforming elements in the finite element method with penalty. *SIAM J. Numer. Anal.*, 10:863–875, 1973.
- [5] C. K. Birdsall and A. B. Langdon. *Plasma Physics via Computer Simulation (Series in Plasma Physics)*. Institute of Physics Publishing, 1991.
- [6] J. H. Bramble and J. T. King. A finite element method for interface problems in domains with smooth boundaries and interfaces. *Adv. Comput. Math.*, 6(2):109–138, 1996.
- [7] Z. Cai, X. Ye, and S. Zhang. Discontinuous Galerkin finite element methods for interface problems: a priori and a posteriori error estimations. *SIAM J. Numer. Anal.*, 49(5):1761–1787, 2011.
- [8] Z. Cai and S. Zhang. Flux recovery and a posteriori error estimators: conforming elements for scalar elliptic equations. *SIAM J. Numer. Anal.*, 48(2):578–602, 2010.
- [9] Z. Chen. *Finite element methods and their applications*. Scientific Computation. Springer-Verlag, Berlin, 2005.
- [10] Z. Chen and J. Zou. Finite element methods and their convergence for elliptic and parabolic interface problems. *Numer. Math.*, 79(2):175–202, 1998.
- [11] S.-H. Chou, D. Y. Kwak, and K. T. Wee. Optimal convergence analysis of an immersed interface finite element method. *Adv. Comput. Math.*, 33(2):149–168, 2010.
- [12] B. Cockburn, G. E. Karniadakis, and C.-W. Shu, editors. *Discontinuous Galerkin methods*, volume 11 of *Lecture Notes in Computational Science and Engineering*. Springer-Verlag, Berlin, 2000. Theory, computation and applications, Papers from the 1st International Symposium held in Newport, RI, May 24–26, 1999.
- [13] J. Douglas, Jr. and T. Dupont. Interior penalty procedures for elliptic and parabolic Galerkin methods. In *Computing methods in applied sciences (Second Internat. Sympos., Versailles, 1975)*, pages 207–216. Lecture Notes in Phys., Vol. 58. Springer, Berlin, 1976.
- [14] R. P. Fedkiw, T. Aslam, B. Merriman, and S. Osher. A non-oscillatory Eulerian approach to interfaces in multimaterial flows (the ghost fluid method). *J. Comput. Phys.*, 152(2):457–492, 1999.
- [15] A. Hansbo and P. Hansbo. An unfitted finite element method, based on Nitsche’s method, for elliptic interface problems. *Comput. Methods Appl. Mech. Engrg.*, 191(47-48):5537–5552, 2002.
- [16] X. He. *Bilinear immersed finite elements for interface problems*. PhD thesis, Virginia Polytechnic Institute and State University, 2009.
- [17] X. He, T. Lin, and Y. Lin. Approximation capability of a bilinear immersed finite element space. *Numer. Methods Partial Differential Equations*, 24(5):1265–1300, 2008.
- [18] X. He, T. Lin, and Y. Lin. Interior penalty bilinear IFE discontinuous Galerkin methods for elliptic equations with discontinuous coefficient. *J. Syst. Sci. Complex.*, 23(3):467–483, 2010.
- [19] X. He, T. Lin, and Y. Lin. The convergence of the bilinear and linear immersed finite element solutions to interface problems. *Numer. Methods Partial Differential Equations*, 28(1):312–330, 2012.
- [20] X. He, T. Lin, and Y. Lin. A selective immersed discontinuous Galerkin method for elliptic interface problems. *Math. Methods Appl. Sci.*, 37(7):983–1002, 2014.
- [21] X. He, T. Lin, Y. Lin, and X. Zhang. Immersed finite element methods for parabolic equations with moving interface. *Numer. Methods Partial Differential Equations*, 29(2):619–646, 2013.
- [22] J. S. Hesthaven and T. Warburton. *Nodal discontinuous Galerkin methods*, volume 54 of *Texts in Applied Mathematics*. Springer, New York, 2008. Algorithms, analysis, and applications.

- [23] T. Y. Hou and X.-H. Wu. A multiscale finite element method for elliptic problems in composite materials and porous media. *J. Comput. Phys.*, 134(1):169–189, 1997.
- [24] R. Kafafy and J. Wang. Whole ion optics gridlet simulations using a hybrid-grid immersed-finite-element particle-in-cell code. *J. Propulsion Power*, 23(1):59–68, 2007.
- [25] D. Y. Kwak, K. T. Wee, and K. S. Chang. An analysis of a broken P_1 -nonconforming finite element method for interface problems. *SIAM J. Numer. Anal.*, 48(6):2117–2134, 2010.
- [26] Z. Li. The immersed interface method using a finite element formulation. *Appl. Numer. Math.*, 27(3):253–267, 1998.
- [27] Z. Li and K. Ito. *The immersed interface method*, volume 33 of *Frontiers in Applied Mathematics*. Society for Industrial and Applied Mathematics (SIAM), Philadelphia, PA, 2006. Numerical solutions of PDEs involving interfaces and irregular domains.
- [28] Z. Li, T. Lin, Y. Lin, and R. C. Rogers. An immersed finite element space and its approximation capability. *Numer. Methods Partial Differential Equations*, 20(3):338–367, 2004.
- [29] Z. Li, T. Lin, and X. Wu. New Cartesian grid methods for interface problems using the finite element formulation. *Numer. Math.*, 96(1):61–98, 2003.
- [30] T. Lin, Y. Lin, R. Rogers, and M. L. Ryan. A rectangular immersed finite element space for interface problems. In *Scientific computing and applications (Kananaskis, AB, 2000)*, volume 7 of *Adv. Comput. Theory Pract.*, pages 107–114. Nova Sci. Publ., Huntington, NY, 2001.
- [31] T. Lin, Y. Lin, and X. Zhang. A method of lines based on immersed finite elements for parabolic moving interface problems. *Adv. Appl. Math. Mech.*, 5(4):548–568, 2013.
- [32] T. Lin, Y. Lin, and X. Zhang. Partially penalized immersed finite element methods for elliptic interface problems. *SIAM J. Numer. Anal.*, 2014. (accepted).
- [33] N. Moës, J. Dolbow, and T. Belytschko. A finite element method for crack growth without remeshing. *Internat. J. Numer. Methods Engrg.*, 46(1):131–150, 1999.
- [34] C. S. Peskin. The immersed boundary method. *Acta Numer.*, 11:479–517, 2002.
- [35] R. Rangarajan and A. J. Lew. Universal meshes: A method for triangulating planar curved domains immersed in nonconforming meshes. *Internat. J. Numer. Methods Engrg.*, 98(4):236–264, 2014.
- [36] W. H. Reed and T. R. Hill. Triangular mesh methods for the neutron transport equation. Tech. Report LA-UR-73-479, Los Alamos Scientific Laboratory, Los Alamos, NM, 1973.
- [37] B. Rivière. *Discontinuous Galerkin methods for solving elliptic and parabolic equations*, volume 35 of *Frontiers in Applied Mathematics*. Society for Industrial and Applied Mathematics (SIAM), Philadelphia, PA, 2008. Theory and implementation.
- [38] B. Rivière, M. F. Wheeler, and V. Girault. Improved energy estimates for interior penalty, constrained and discontinuous Galerkin methods for elliptic problems. I. *Comput. Geosci.*, 3(3-4):337–360 (2000), 1999.
- [39] S. Vallaghé and T. Papadopoulo. A trilinear immersed finite element method for solving the electroencephalography forward problem. *SIAM J. Sci. Comput.*, 32(4):2379–2394, 2010.
- [40] J. Wang, X. He, and Y. Cao. Modeling Electrostatic Levitation of Dust Particles on Lunar Surface. *IEEE Transactions on Plasma Sciences*, 36(5):2459–2466, 2008.
- [41] M. F. Wheeler. An elliptic collocation-finite element method with interior penalties. *SIAM J. Numer. Anal.*, 15(1):152–161, 1978.
- [42] X. Zhang. *Nonconforming Immersed Finite Element Methods for Interface Problems*. ProQuest LLC, Ann Arbor, MI, 2013. Thesis (Ph.D.)–Virginia Polytechnic Institute and State University.